J. Fluid Mech. (1982), *vol.* 122, *pp.* 295-314
Printed in Great Britain

On the structure of turbulent channel flow

By ARNE V. JOHANSSON AND P. HENRIK ALFREDSSON
Department of Mechanics, The Royal Institute of Technology,
S-100 44 Stockholm, Sweden

(Received 1 September 1981 and in revised form 26 January 1982)

Hot-film measurements of the streamwise velocity component were carried out in a fully developed turbulent water-channel flow for three different Reynolds numbers (13800, 34600 and 48900). The results for the first four statistical moments complement and extend the results from previous studies of turbulent channel flow. The VITA variance technique was employed to detect deterministic events in the streamwise velocity. It was demonstrated that the VITA technique has a band-pass-filter character. The number of events detected was found to decrease exponentially with the threshold level and the events occupy a wide range of timescales. This makes it impossible to define one unique frequency of occurrence or one unique duration of the events. However, by using this technique information was obtained on the amplitude and timescale distributions of the events. The characteristic features of the conditional averages were found to be related to the skewness and flatness factors.

1. Introduction

Fully developed turbulent channel flow has been studied by several investigators during the last three decades (e.g. Clark 1968; Comte-Bellot 1965; Eckelmann 1974; Kreplin 1976; Laufer 1951; Zarič 1975). In the present study measurements are presented for three different Reynolds numbers with a ratio of nearly 4 to 1. Water was used as the working fluid, and the streamwise velocity component was measured with the use of a single hot-film probe. Water has the advantage over air in that effects of heat conduction from the probe to the wall are small.

Several methods have been devised to sort out organized structures from turbulent signals measured at one or more fixed points in the flow. When referring to such structures, the term event, instead of for example burst, will be used in the following. Rao, Narasimha & Badri Narayanan (1971) employed a complex scheme to identify events from the band-pass-filtered streamwise velocity signal, while the method of Willmarth & Lu (1972) detects events when the low-pass-filtered u-signal at $y^+ = 15$ is below a pre-set value. The scheme of Blackwelder & Kaplan (1976), usually referred to as the VITA technique, utilizes the short-time variance of the streamwise velocity signal at $y^+ = 15$. The short-time variance is a localized (in time) measure of the turbulent activity, and when it exceeds a given threshold level an event is said to occur. The uv-signal (as well as the short-time variance of u) has an intermittent character, which is made use of by Sabot & Comte-Bellot (1976) to detect events. Wallace, Brodkey & Eckelmann (1977) devised a pattern-recognition scheme and found events characterized by a relatively weak deceleration of the flow followed by

a strong acceleration. These u-signal patterns were found at all positions throughout the flow field. For a more detailed description of the above-mentioned and other related investigations the reader is referred to the review articles of Willmarth (1975) and Antonia (1981).

In §3.1 are presented measurements of mean velocity, turbulence intensity, skewness and flatness that complement and extend the results of previous channel-flow studies. The main portion of this study is, however, devoted to the detection of events in the streamwise velocity signal with the use of the VITA technique. The detection of events was carried out at various distances from the wall and for a wide range of values of the parameters involved in the detection criterion. The results, presented in §3.2, show for example that the VITA technique has a band-pass-filter character and that the features of the conditional averages of u are related to the skewness and flatness factors.

2. Experimental arrangement

2.1. *Experimental facility and measurement technique*

The experiments were carried out in the water tunnel (see figure 1) at the Department of Mechanics of the Royal Institute of Technology, Stockholm. The tunnel is of a continuous-flow type and has a velocity range of about 0·15–5 m/s. The measurements were carried out 63 channel heights from the inlet of the 6 m long test section, which is made of Plexiglas and has a width of 400 mm and a height of 80 mm. The DISA M01 anemometer system and boundary-layer-type fibre film probes (DISA model R15) were used for the measurements of the streamwise velocity component. The probes were run at constant temperature with an overheat of 16 °C. The diameter and length of the sensing element of the probe are 0·070 and 1·25 mm respectively. In the present study the maximum centreline velocity was 0·61 m/s, which is low enough to avoid vortex shedding from these probes. A traversing mechanism with a resolution of 5 μm was used to position the probe. The position closest to the wall was determined by a microscope technique with an accuracy of 0·05 mm. A more detailed description of the water tunnel is given by Johansson & Alfredsson (1981).

The hot-film probes were calibrated in a submerged water jet. The calibration apparatus and procedure are described in detail by Fahlgren, Johansson & Alfredsson (1981). The transformation from voltage to velocity was done digitally with the use of a calibration curve consisting of two parts, with a condition of continuity at the matchpoint located at about 10 cm/s. The maximum error (in the velocity) could thereby be kept to less than 2 %. A King's law expression was used in the upper velocity range. In the lower range an expression of the form

$$U = k_1(E^2 - E_0^2)^{1/n} + k_2(E - E_0)^{\frac{1}{2}} \tag{1}$$

was used, where E and E_0 are the anemometer output voltages at the velocities U and zero respectively, and k_1, k_2 and n are constants to be adjusted for best fit of (1) to the calibration data. The second term in (1) is related to the effects of natural convection, which become important at low velocities..

For hot-film measurements in water it is of utmost importance to use clean water of constant temperature. A filtering and temperature control system was used to remove particles larger than 5 μm and to keep the water temperature constant to

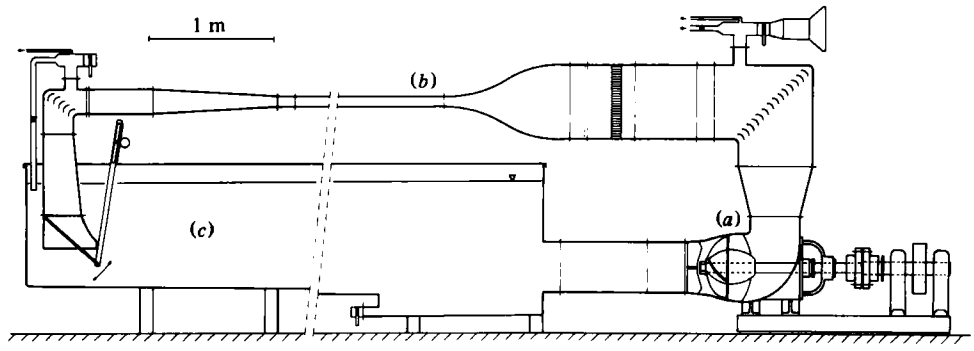

FIGURE 1. The water tunnel: (*a*) pump, (*b*) test section, (*c*) water reservoir.

within $\pm 0{\cdot}03$ °C. The anemometer voltage was compensated for small temperature variations by the method used by Fahlgren *et al.* (1981). However, this compensation was always less than 0·4 % of the velocity.

For each measurement point 230000 samples of the anemometer output signal were collected (after subtracting a d.c. voltage using the DISA D25 signal conditioner) through the 12-bit A/D converter of a DEC MINC system (PDP11/23), and stored on floppy disk. The time between consecutive samples was chosen as about half the viscous timescale. For the lowest velocity this corresponds to a sampling time of about 20 min at each measuring point. The probability density distributions of the anemometer signal were computed from the time series and transformed to the probability density distributions of the streamwise velocity by using the calibration curve. The different moments, i.e. mean velocity, r.m.s. velocity, skewness and flatness factors, were then calculated from these distributions. Assembler programs were used for most of the numerical work.

2.2. *The VITA technique*

Blackwelder & Kaplan (1976) developed the VITA technique to detect the occurrence of events associated with the turbulence production. This method uses the intermittent character of the short-time variance of the streamwise velocity. It is assumed that peaks in the short-time variance signal correspond to such events. The short-time variance (or the VITA variance) of the fluctuating streamwise velocity component u is defined as

$$\mathrm{var}\,(t,T) = \frac{1}{T}\int_{t-\frac{1}{2}T}^{t+\frac{1}{2}T} u^2(s)\,ds - \left(\frac{1}{T}\int_{t-\frac{1}{2}T}^{t+\frac{1}{2}T} u(s)\,ds\right)^2. \tag{2}$$

When T becomes large the second term on the right-hand side of (2) tends to zero, and twice the long-time average of the turbulent energy from the u-component (per unit mass), i.e. u^2_{rms}, is obtained. As T approaches zero the two terms on the right-hand side of (2) become identical, so that the short-time variance vanishes. As can be seen from a simple example there is a close relation between the timescales contributing to the short-time variance and the integration time. In figure 2 the short-time variance for a single period of a sine wave is plotted versus the integration time. A type of band-pass-filter character is observed, with the maximum of the short-time variance located at an integration time of 72 % of the period. To examine the influence

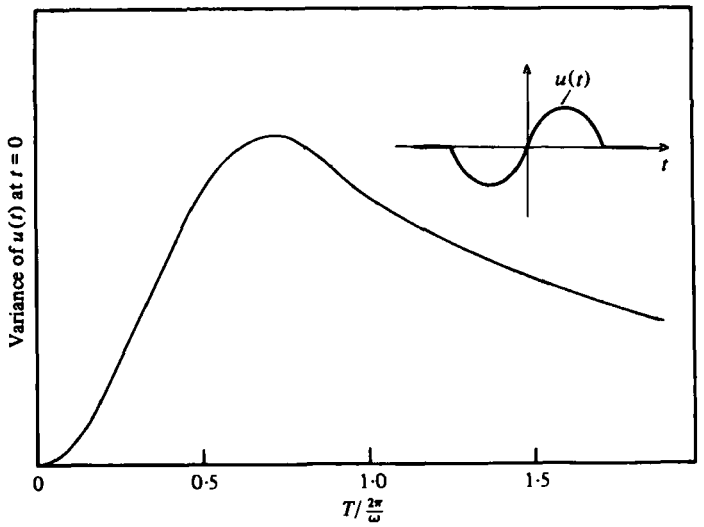

FIGURE 2. The short-time variance (at $t = 0$) of $u(t) = \sin \omega t$ $(-\pi/\omega < t < \pi/\omega)$, 0 (otherwise).

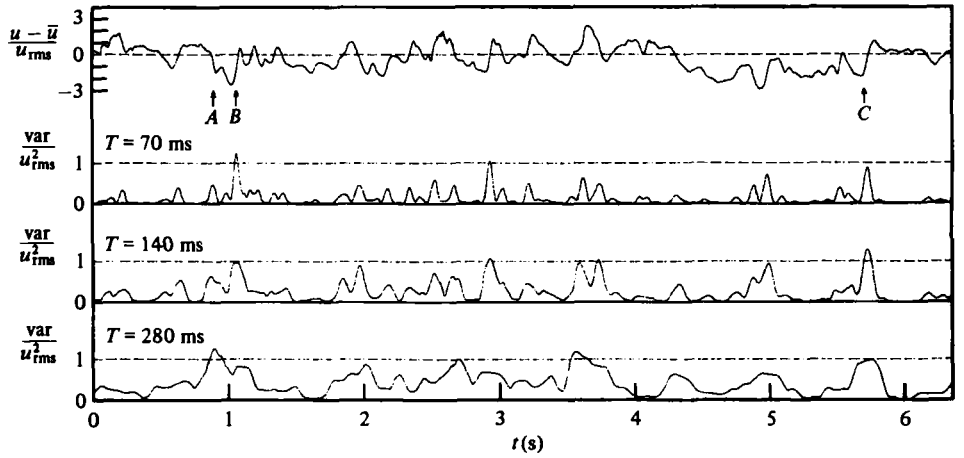

FIGURE 3. Velocity signal and corresponding short time variance functions for three different integration times; $Re = 13\,800$, $y^+ = 12{\cdot}9$.

of the test-signal shape, a triangle wave was substituted for the sine wave. A slightly modified short-time variance was obtained, and the maximum was instead found for an integration time of 78 % of the period.

The detection criterion used by Blackwelder & Kaplan (henceforth referred to as the VITA technique) states that an event occurs when the short-time variance exceeds ku^2_{rms}, where k is the chosen threshold level. The reference time is taken as the mid-point of the event. Once the reference times have been determined, a conditional average of the u-signal can be calculated as

$$\langle u(\tau) \rangle = \frac{1}{N} \sum_{j=1}^{N} u(t_j + \tau),$$

where N is the number of events and τ is a time relative to the reference time t_j.

Reynolds number $U_{CL}\,2b/\nu$	13800	34600	48900
U_{CL} (m/s)	0·174	0·461	0·615
U_{CL}/u_τ	20·6	23·0	23·7
Viscous lengthscale $l_* = \nu/u_\tau$ (mm)	0·119	0·053	0·039
Viscous timescale $t_* = \nu/u_\tau^2$ (ms)	14·1	2·65	1·48
Outer timescale $t_0 = b/U_{CL}$ (ms)	230	86·7	65·0
Additive constant in the logarithmic velocity law	5·8	5·5	5·0

TABLE 1. Characteristics of the channel flows

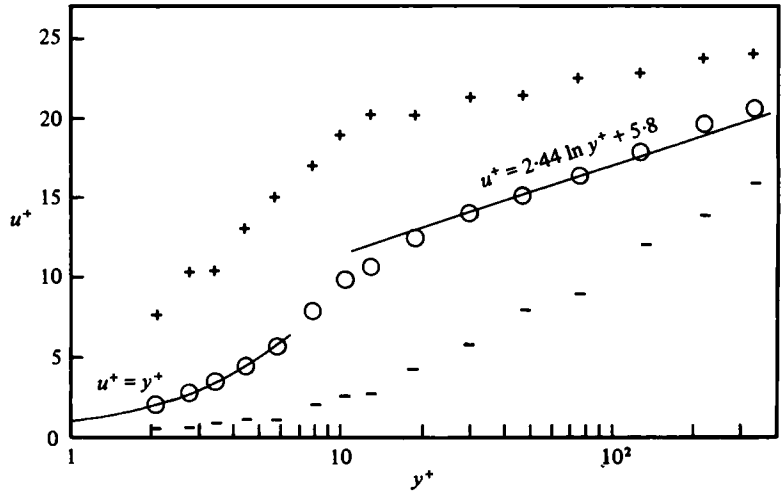

FIGURE 4. Distributions of measured maximum (+), minimum (−) and mean velocities (○); Re = 13800.

Figure 3 shows a portion of the u-signal and the corresponding variance functions calculated for three different integration times (corresponding to 5, 10 and 20 viscous time units). The variance functions have a rather intermittent appearance, especially for short integration times. The band-pass-filter character of the VITA technique is well illustrated in this figure. For instance at A the variance function has a peak, which increases with increasing integration time. It corresponds to a rather slow decrease of the u-velocity. However, this deceleration is followed by a rapid acceleration at B, which gives the variance function its highest value for the shortest integration time. At C the acceleration of the flow has a timescale somewhere in between the other two, and the variance function has its highest value for an intermediate integration time.

3. Results

3.1. *Long-time-average results*

Measurements were carried out at three different Reynolds numbers, namely 13800, 34600 and 48900, based on centreline velocity U_{CL}, channel height $2b$ and fluid viscosity ν. Some characteristic parameters of these flows are given in table 1.

The question as to whether the flow is fully developed or not will first be addressed. Comte-Bellot (1965) carried out extensive experiments, studying the downstream

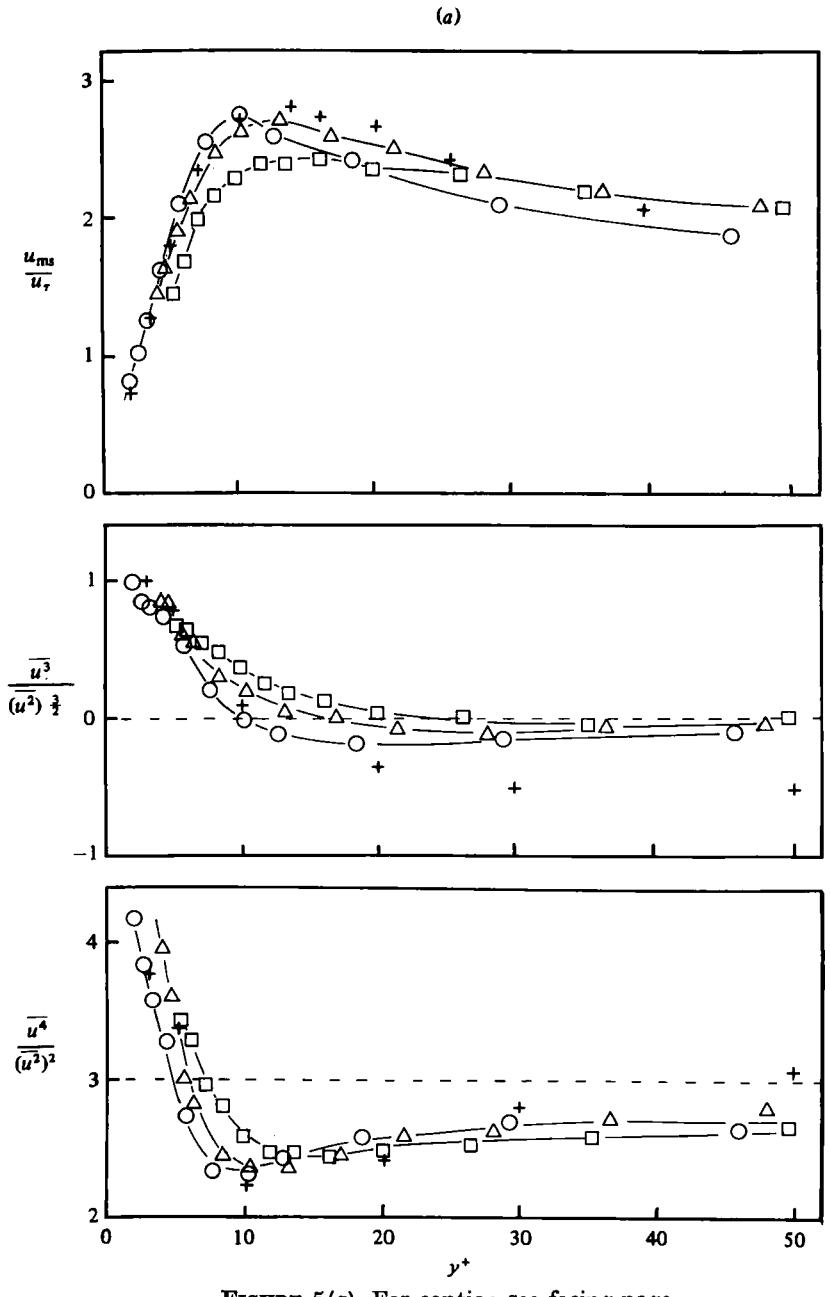

FIGURE 5(a). For caption see facing page.

development of turbulent channel flow. Her experiments showed that a good characterization of the stage of development could be made, based on the values of the skewness and flatness factors on the channel centreline. A channel flow that is not fully developed will show a large negative value of the skewness and a large positive value of the flatness factor. Comte-Bellot found that the fully developed regime, where all statistical moments are independent of the downstream distance, was

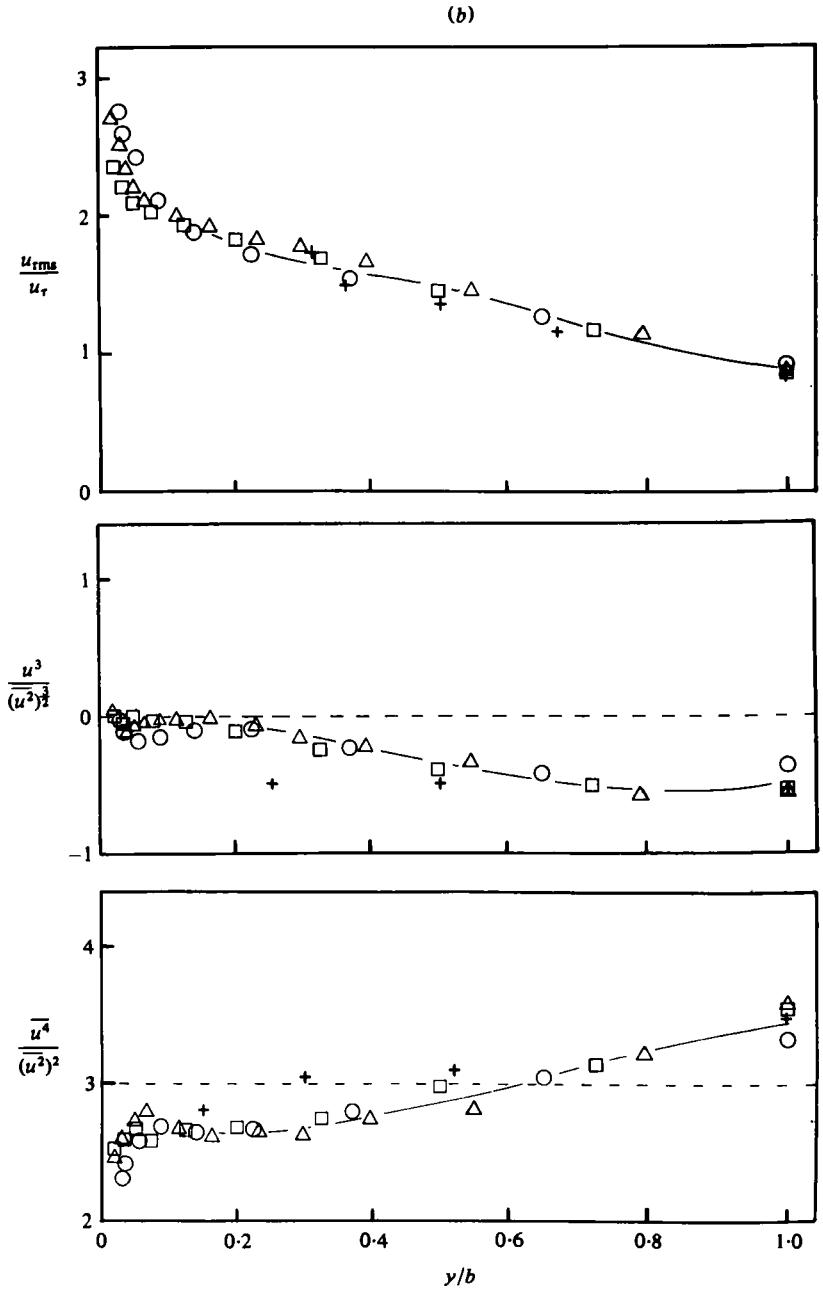

FIGURE 5. Distributions of the streamwise turbulence intensity, skewness and flatness: (*a*) inner region, (*b*) outer region. ○, Re = 13800; △, 34600; □, 48900; +, Kreplin (1976), Re = 7700.

established about 60 channel heights downstream of the inlet. The present measurements were carried out 63 channel heights from the inlet, and as reported by Johansson & Alfredsson (1981) the variation of the skewness and flatness factors on the centreline is negligible beyond $x/2b = 57$.

In figure 4 the mean-velocity distribution for the lowest Reynolds number (13800)

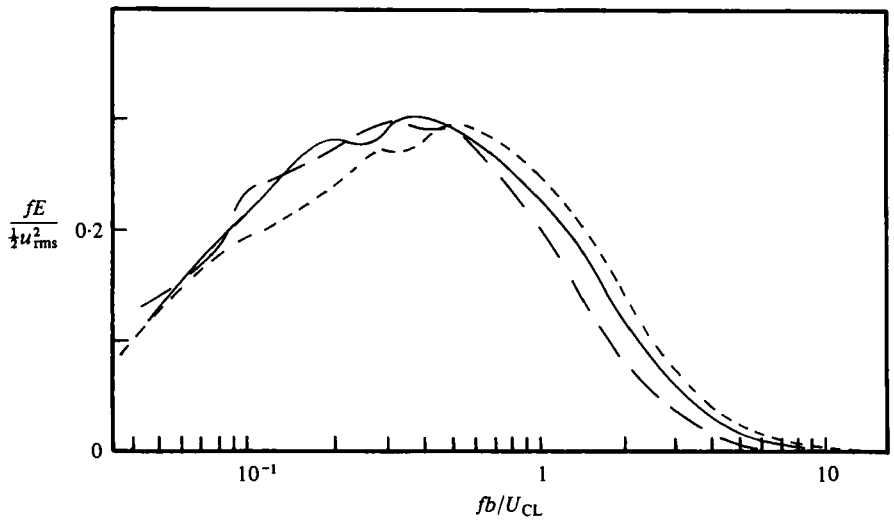

FIGURE 6. Frequency spectra of the streamwise velocity component; $y^+ = 13$. — —, $Re = 13\,800$; ——, 34 600; - - - -, 48 900.

is presented in the standard form of u^+ *vs.* y^+ ($u^+ = U/u_\tau$, $y^+ = y/l_*$). For this Reynolds number the friction velocity could be determined from the slope of the mean-velocity profile in the viscous sublayer. For the higher Reynolds numbers the friction velocities were determined from the condition of best fit to the logarithmic velocity law with von Kármán's constant equal to 0·41. The results show a slight reduction, with increasing Reynolds number, of the additive constant in the logarithmic velocity law (table 1). Also included in figure 4 are the maximum and minimum velocities measured at each point, showing the large span of velocities present.

The turbulence intensity has its maximum value at about $y^+ = 12$ (figure 5) where also the span of measured velocities is largest as seen in figure 4. The highest velocity at this point is about as large as the mean velocity at the centreline, and the lowest is about $u^+ = 2$. The maximum in turbulence intensity, however, becomes less pronounced and is also shifted to slightly higher y^+ values with increasing Reynolds number. This trend is consistent with the data of Laufer (1951) and Comte-Bellot (1965). As shown by Zarič (1972) large differences between various studies are at hand for measurements of u_{rms}/u_τ in the near-wall region ($y^+ < 50$), which cannot be attributed solely to Reynolds-number effects. In most studies prior to 1970 non-linearized anemometer signals were used, and various corrections to the measured quantities were applied. This is of course more questionable than to use analog or digital linearization of the anemometer signal. It is also worth mentioning that measurements close to the wall seem to be more influenced by cooling from the wall for hot wires in air than for hot films in liquids. For measurements in air the thermal conductivity of the test-section wall is usually much higher than that of air. The wall will hence act as a heat sink. This effect will also be enhanced by the high overheat temperatures usually employed in air (≈ 200 °C). The effects of this additional cooling on measurements of mean and fluctuating quantities are rather uncertain.

The skewness and flatness factors, presented in figure 5, show a slight Reynolds-number dependence in the near-wall region. The data of Kreplin (1976) ($Re = 7700$),

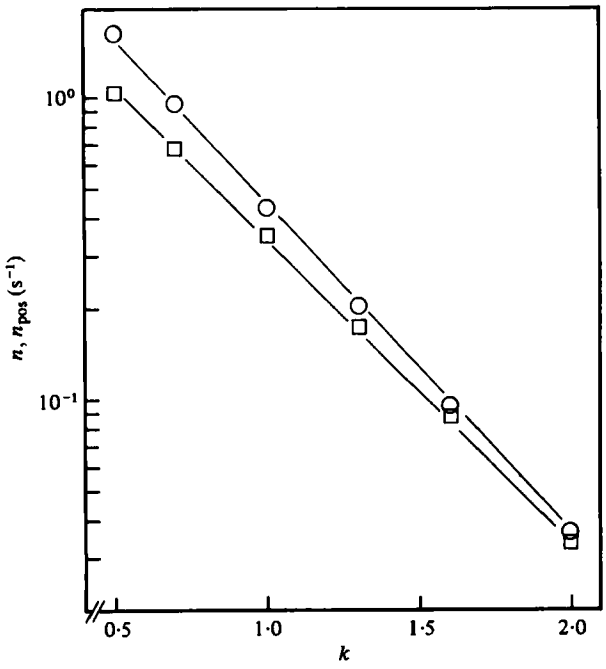

FIGURE 7. Total number of events (○) and number of events with positive slope (□) detected per unit time as function of the threshold level; $Re = 13800$, $T^+ = 10{\cdot}7$, $y^+ = 12{\cdot}9$.

also included in figure 5, are consistent with the present data close to the wall. In the outer region, however, there are differences that may be due to Reynolds-number effects. They may also be due to for example the different development lengths of the two channels ($x/2b = 32$ for Kreplin and $x/2b = 63$ for the present study).

Frequency spectra were calculated by means of standard FFT routines. The data are presented as fE, i.e. the frequency times the energy density function, in a linear scale, versus f in a logarithmic scale. The ordinate is normalized so that the total non-dimensional energy is unity. Spectra for the three Reynolds numbers at $y^+ \simeq 50$ and further out collapse when the frequency is scaled with the outer timescale. This scaling was also found by Perry & Abell (1975) to be appropriate in the outer region of turbulent pipe flow. However, the outer scaling works less well with decreasing distance from the wall. At $y^+ = 13$ neither outer (figure 6) nor inner scaling works satisfactorily. In figure 6 a clear Reynolds-number trend is seen in the high-frequency range. Not even at the edge of the viscous sublayer ($y^+ = 5$) do the spectra for all three Reynolds numbers collapse with inner scaling.

3.2. *Short-time average results*

Data from the measurements presented in §3.1 were also analysed using the VITA technique. As will be shown in the following, the number of events n detected per unit time varies strongly with the threshold level k and the integration time T. When scaled with outer or inner flow variables the integration time will be denoted by T_0 and T^+ respectively. Two distinctly different types of events can be distinguished, corresponding to accelerations and retardations. Those with increasing velocity at

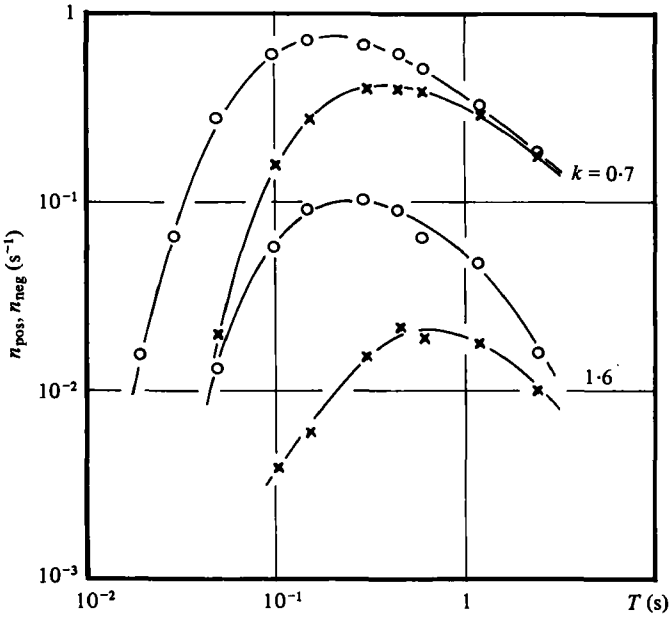

FIGURE 8. Number of events with positive slope (○) and with negative slope (×) detected per unit time as function of the integration time; $Re = 13800$, $y^+ = 12{\cdot}9$.

the reference time will also be referred to as having positive slope. The number of such events detected per unit time will be denoted by n_{pos}. The corresponding quantity for the events with negative slope is denoted by n_{neg}. A large portion of the results presented in the following were obtained for y^+ positions of about 13, where the turbulence production and intensity are largest.

The number of events detected decreases exponentially with increasing threshold level for the case in figure 7 ($y^+ = 12{\cdot}9$). An increase in k from 0·5 to 2·0 results in a decrease of n by a factor of more than 40. Also plotted is the number of events corresponding to accelerations. The two lines, representing n and n_{pos}, merge at high threshold levels. This indicates that nearly all events with very large amplitudes, typically several times the long-time r.m.s. value, correspond to acceleration of the flow. As the mean amplitude of all detected events is approximately proportional to the square root of the threshold level used (as will be supported by results presented later) information about the amplitude distribution of the events is acquired from plots such as those in figure 7. The exponential decrease of n with increasing k was found for all y^+ values, integration times and Reynolds numbers studied. The rate of decrease, however, varies with for example the distance from the wall. Using the uv-quadrant method, Sabot & Comte-Bellot (1976) also found that the number of events detected decreases exponentially with the threshold level.

The predominance of events corresponding to acceleration over those corresponding to retardation of the flow was found in all cases studied for large k-values. The same predominance is also found for small integration times, which is illustrated in figure 8. Thus the most rapid events nearly always correspond to accelerations. For no values of T and k investigated do the events with negative slope dominate. The curves $n_{pos}(T)$ (or $n_{neg}(T)$) are similar in shape for different k-values, and the maxima

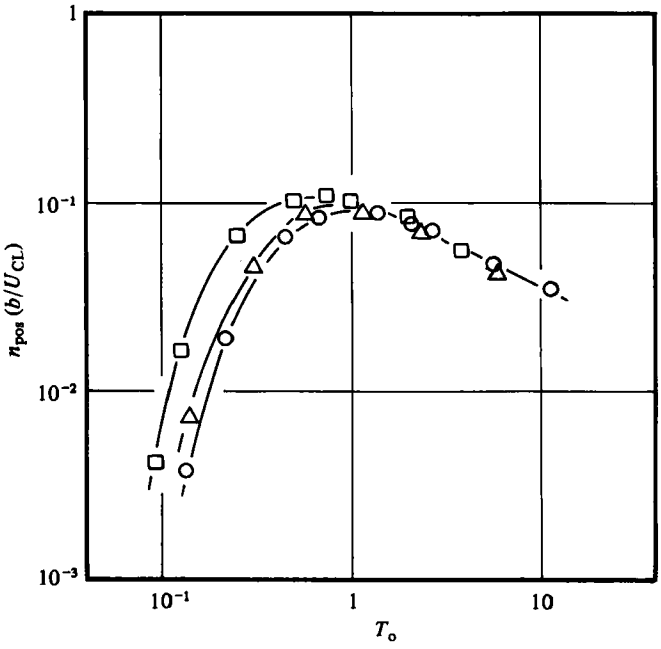

FIGURE 9. Number of events with positive slope versus the integration time, with outer scaling; $k = 1{\cdot}0$, $y^+ = 13$. ○, $Re = 13800$; △, 34900; □, 48900.

are not very distinct, which implies that the events occupy a wide range of timescales for all threshold levels. The relation between T and the duration of the events will become evident from the conditional averages presented later. Information is thus obtained on the timescale distribution of the events from plots as those in figure 8. For this case ($y^+ = 13$) the T-value for which n_{pos} has its maximum corresponds to about 16 viscous time units or about 1·0 in outer units and is only about one-third of that for which n_{neg} has its maximum. This means that the timescale for the retardations is typically several times as large as the timescale for the accelerations. This is probably related to the large positive values of the skewness factor of du/dt as measured by Comte-Bellot (1965) and also to the shape of the u-signal patterns found by Wallace *et al.* (1977). These patterns are characterized by a relatively slow retardation followed by a rapid acceleration. A comparison between the curves in figure 8 and the corresponding power spectrum in figure 6 reveals that most of the turbulent energy is found in a frequency range that corresponds to timescales for which many events are detected.

In figure 9, curves representing $n_{pos}(T)$ (at $y^+ = 13$) are plotted for the three different Reynolds numbers specified in § 3.1. For integration times longer than about one outer time unit the curves collapse when outer scaling is applied. This was found to be true also at other y^+ positions examined (i.e. $y^+ > 5$). This indicates that both the duration and the frequency of occurrence of events with a typical timescale larger than roughly one outer time unit may be governed by outer flow variables. The curves $n_{pos}(T)$ collapse better with increasing distance from the wall when outer scaling is used. However, neither outer nor inner scaling makes the curves collapse over the whole range of integration times for positions close to the wall (e.g. at $y^+ = 5$ and

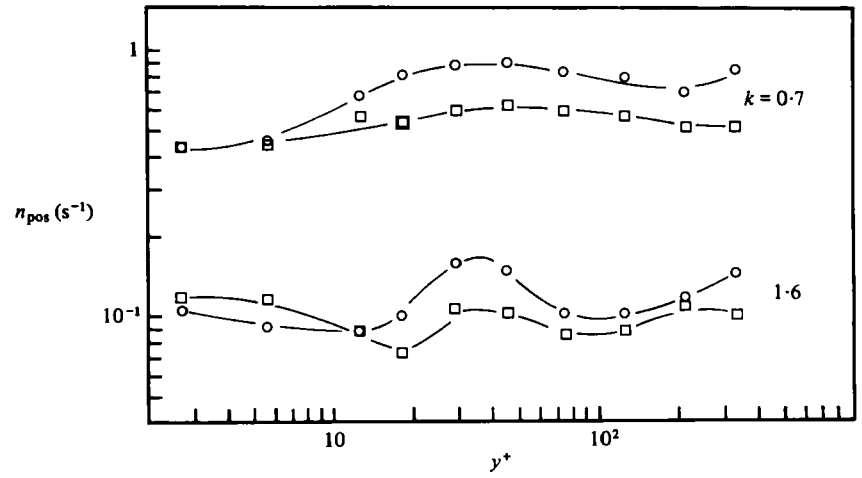

FIGURE 10. Distribution of the number of events with positive slope across the channel; Re = 13800. ○, T^+ = 10; □, T_0 = 2·0.

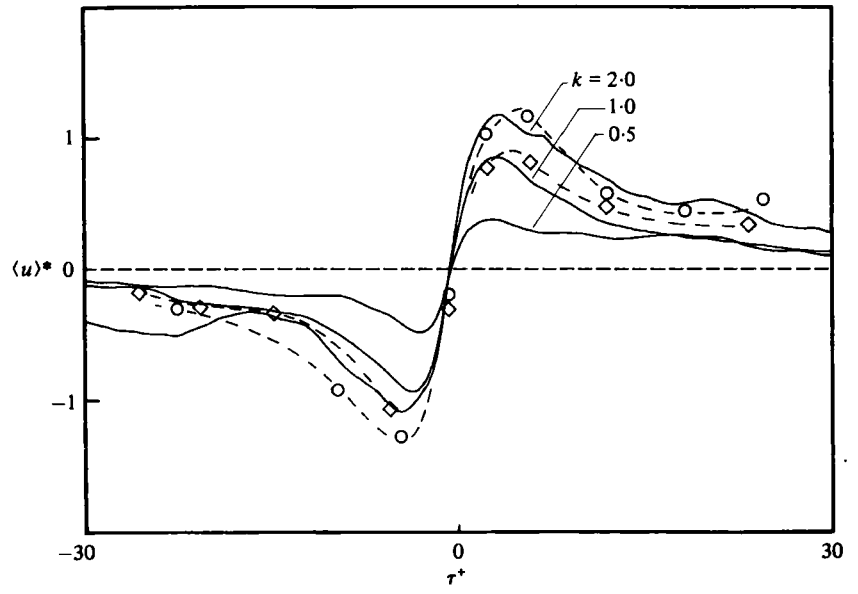

FIGURE 11. Conditional averages constructed from all events detected for three different threshold levels; Re = 13800, T^+ = 10·7, y^+ = 12·9. Data from Blackwelder & Kaplan (1976) are included with T^+ = 10, y^+ = 15. ◇, k = 1·0; ○, 2·0.

y^+ = 13). This situation should be compared with the one encountered for the scaling of frequency spectra (see §3.1). For the low Reynolds number, with T^+ = 10, n_{pos} varies with a factor of about two across the channel (figure 10). For longer integration times, however, n_{pos} becomes more evenly distributed. This may be related to the findings of Bullock, Cooper & Abernathy (1978) from measurements in a turbulent pipe flow. They showed that the low-frequency components (corresponding to several outer time units) of the u-signal are highly correlated over large distances normal to the wall.

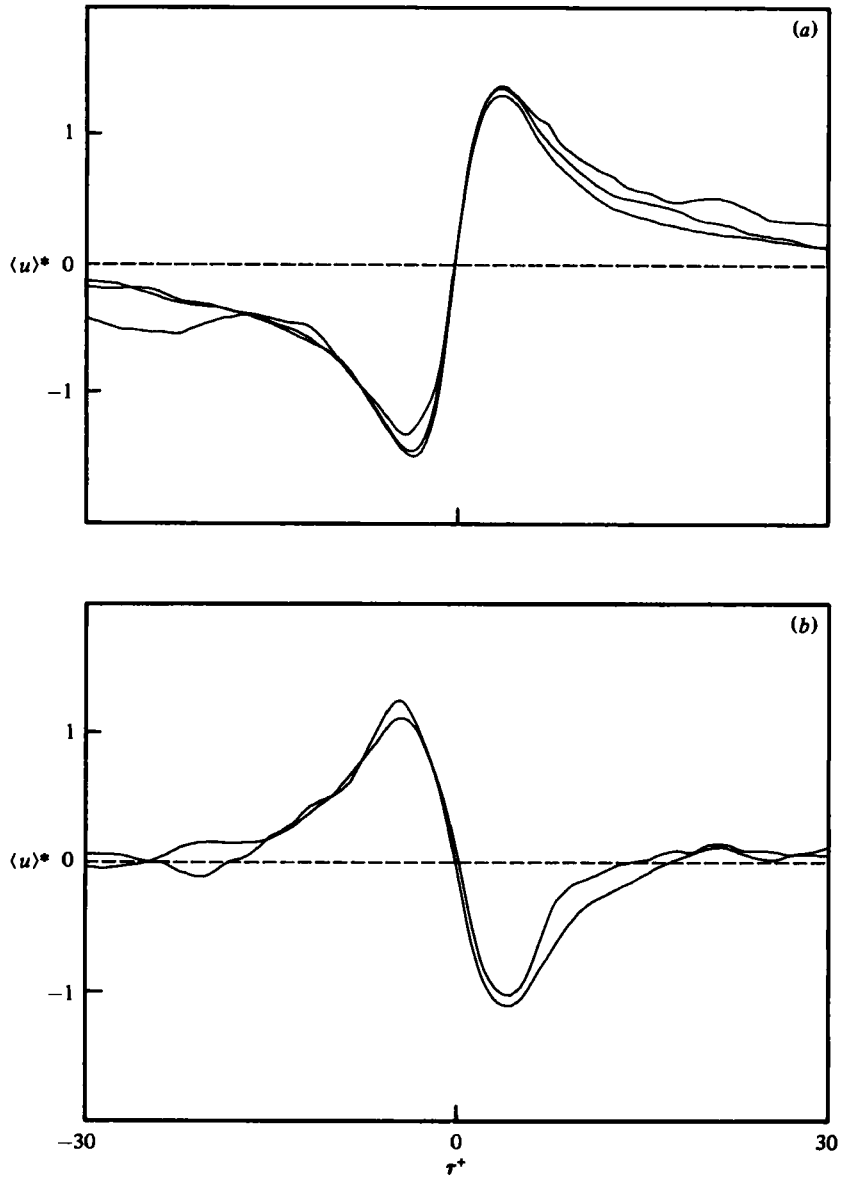

FIGURE 12. The data of figure 11 separated into events with (*a*) positive slope, (*b*) negative slope.

The conditional average of u is computed as the ensemble average of portions of the u-signal centred around their respective reference times (see §2.2). Following Blackwelder & Kaplan (1976), the conditional averages of u are made non-dimensional with $(ku_{\mathrm{rms}}^2)^{\frac{1}{2}}$ and are denoted by $\langle u\rangle^*$ (the time co-ordinate is scaled with the viscous timescale). The three curves in figure 11 represent the conditional averages of all events for threshold levels 0·5, 1·0 and 2·0 (for $Re = 13\,800$ at $y^+ = 12{\cdot}9$). Also included are results from Blackwelder & Kaplan (1976) for k-values 1·0 and 2·0. The agreement between the two sets of results is fairly good. The conditional averages

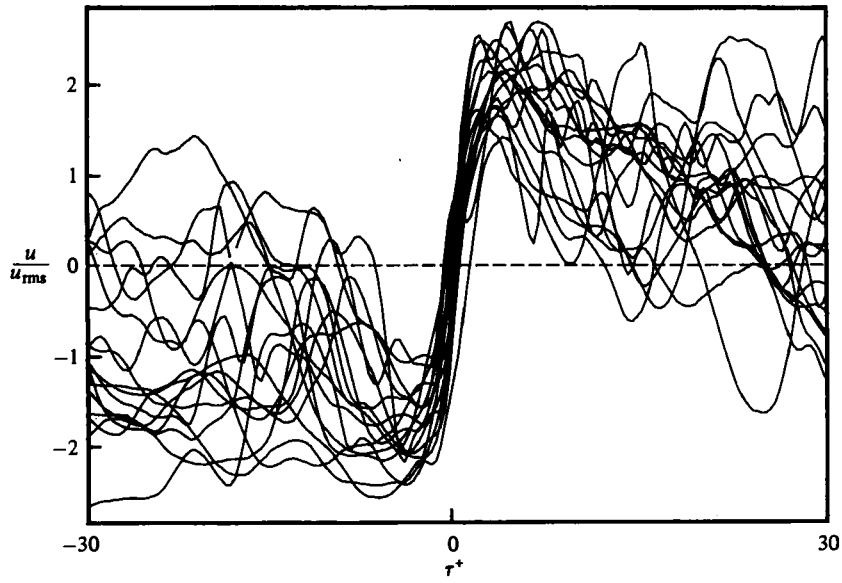

FIGURE 13. 17 single events for the case in figure 12(*a*) with $k = 2{\cdot}0$.

show an increasing velocity at the reference time, which implies that the events with positive slope dominate. This is especially pronounced for large k-values. The conditional averages (for the present study) in figure 11 are based on 1637, 432 and 37 events for the threshold levels 0·5, 1·0 and 2·0, respectively. The velocity scaling applied does not make the curves for different k-values collapse when k is varied over this range. As already noted, however, there are two distinctly different types of events, corresponding to accelerations and retardations. Construction of the ensemble averages from all events as in figure 11 then gives a somewhat misleading picture, because the events with negative slope have an attenuating effect on the amplitude of the ensemble averages. Since the distribution between events with positive and negative slopes changes with k (as seen in figures 7 and 8) the velocity scaling of the conditional averages of all events can only be expected to have limited success. An alternative approach, near at hand, is to treat the two types of events separately. The conditional averages of all events with positive slope are shown in figure 12(*a*). The corresponding averages for negative slopes are found in figure 12(*b*), where, however, the highest threshold level has been excluded because of the small number of events (only three) detected. The averages are now seen to collapse well for both types of events, with the same scaling as used in figure 11. For this reason the curves for different k-values are not labelled. All events with amplitudes corresponding to higher k-values than the threshold level used are included in the ensemble average. However, as the number of events decreases exponentially with k (figure 7) only a small interval of amplitudes (and timescales related to the integration time) will contribute significantly to the ensemble average. This explains why the data collapse with the above-mentioned scaling. The amplitudes of the conditional averages also become larger when the two types of events are treated separately. The collapse of the conditional averages indicates that the mean amplitude of the detected events is proportional to the square root of the threshold level, which indeed is to be expected from

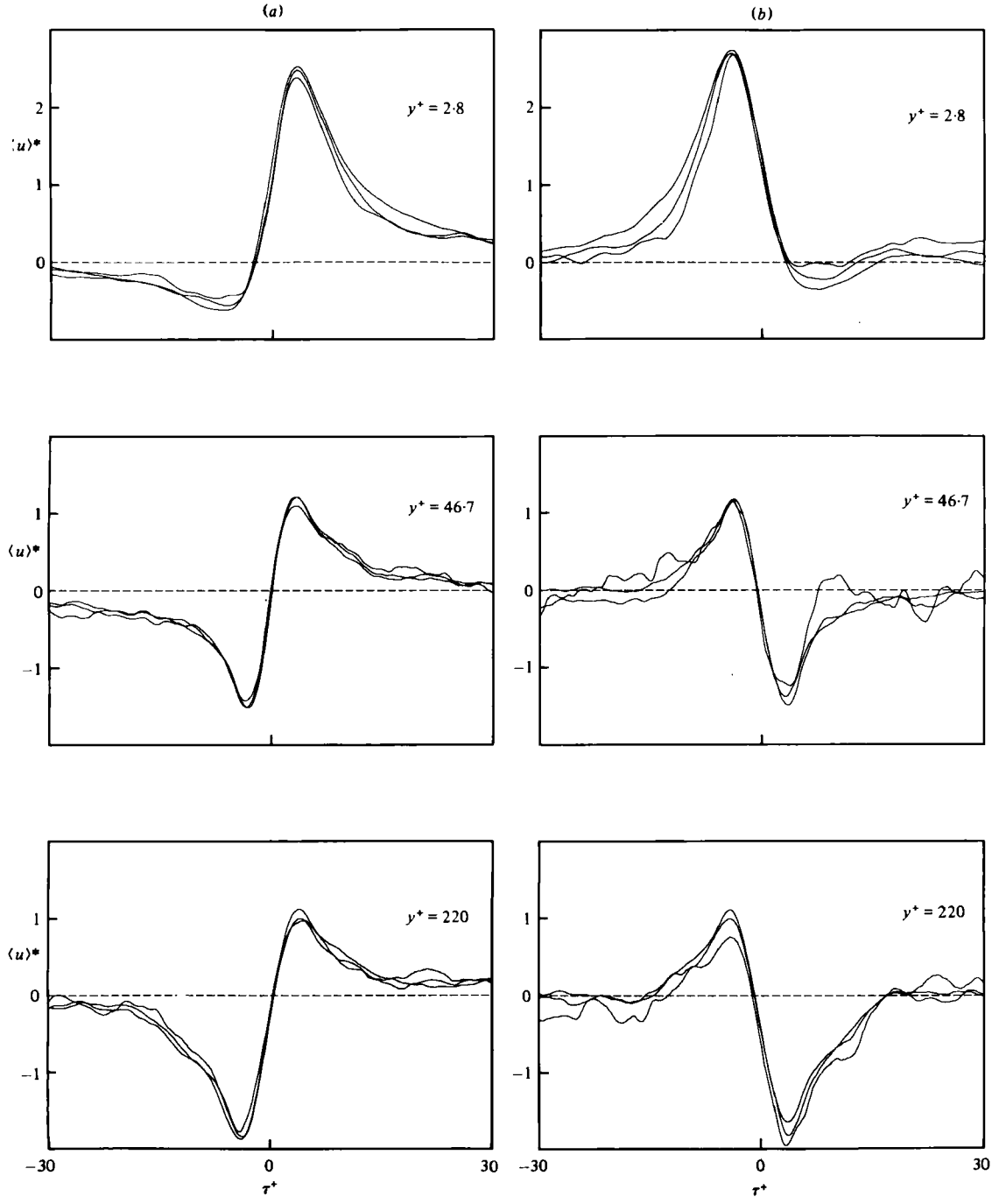

FIGURE 14. Conditional averages for events with (*a*) positive slope and (*b*) negative slope; $Re = 13800$, $T^+ = 10{\cdot}7$, $k = 0{\cdot}5$, $1{\cdot}0$ and $2{\cdot}0$.

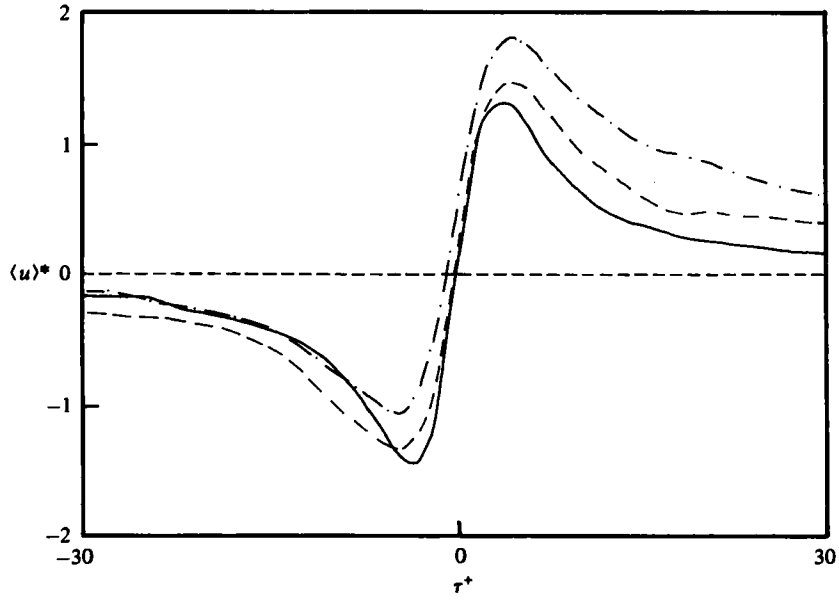

FIGURE 15. Conditional averages at $y^+ = 13$ for three different Reynolds numbers; $T^+ = 10$. ——, $Re = 13800$; — —, 34600; · - · - · - ·, 48900.

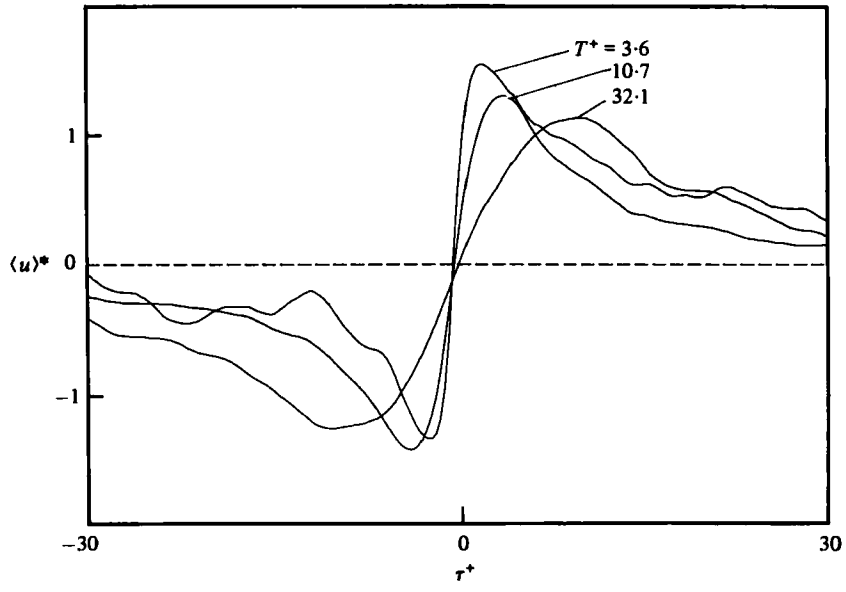

FIGURE 16. Conditional averages for events having positive slope for different integration times; $Re = 13800$, $y^+ = 12{\cdot}9$, $k = 1{\cdot}0$.

the definitions of the short time variance and the threshold level. The amplitude ('peak to peak') for $k = 2{\cdot}0$ is found in figure 12(a) to be nearly four times the long-time r.m.s. value of u. To give a picture of the appearance of single events figure 13 shows 17 different realizations that are included in the ensemble average for $k = 2{\cdot}0$ in figure 12 (a).'

In figures 14(*a*, *b*) the conditional u-averages are shown for y^+ values of 2·8, 46·7 and 220 for events with positive and negative slope. The events are detected at the respective position. In the viscous sublayer the ensemble averages are clearly shifted towards positive values, whereas they are approximately symmetric (around the long-time mean value) at $y^+ = 12{\cdot}9$ (see figure 12*a*). Further out they become shifted towards the negative side. This is in close correspondence with the behaviour of the skewness factor, which is positive close to the wall, changes sign at about $y^+ = 10$, and becomes negative further out (see figure 5). There also seems to be a correspondence between the maximum deviation of the ensemble average from the long-time mean value, and the flatness factor. The highest value of the flatness factor is obtained in the viscous sublayer, where the maximum deviation (from the long-time mean value) of the ensemble averages is also greatest. As would also be expected from the conditional averages (with the same reasoning) the flatness factor at $y^+ = 220$ ($y/b = 0{\cdot}65$) is greater than at $y^+ = 46{\cdot}7$. Furthermore, it is observed that the velocity scaling used collapses the conditional averages well at all positions. Conditional averages of u for the other Reynolds numbers were found to be similar to those for the low Reynolds number. In figure 15 the conditional averages at y^+ values of about 13 are compared for different Reynolds numbers. They are similar in shape, but shifted to the positive side with increasing Reynolds number in accordance with the positive trend of the skewness factor (figure 5).

Conditional averages calculated for three different integration times are shown in figure 16. The influence of the integration time on the curves is clear, which again demonstrates the close relation between the integration time used and the timescales filtered out.

4. Discussion

Several studies have been carried out in order to investigate the structure of turbulent channel flow. However, measurements of higher statistical moments are scarce. Data for the skewness and flatness factors over a fairly wide Reynolds-number range are presented by Comte-Bellot (1965) and in the present paper. Our data exhibit a Reynolds-number trend in the near-wall region that is in contrast with the data of Comte-Bellot. However, our low-Reynolds-number case shows good agreement with the data of Kreplin (1976) ($Re = 7700$) in this region. The differences may be due partly to different measurement techniques (analog versus digital). Spatial averaging over the probe may also affect the measurements if the probe length is of the same size or larger than the smallest spanwise turbulence scales. To avoid this problem the probe needs to be of smaller physical dimensions at higher Reynolds numbers. In order to verify (or test) the apparent Reynolds-number trend in the data, measurements should be taken with probes of various sizes. Such measurements are currently under way.

The interpretation of results obtained with the various detection schemes mentioned in §1, is a non-trivial matter, and the relation between the parameters involved and the physical properties of the events detected is not always clear. Almost all methods use a threshold level of some sort to identify events. In the VITA technique an integration time is also involved in the detection criterion. The relation between the integration time and the typical timescale (or duration) of the events is illustrated

in for example figures 12 and 16. The slope (du/dt at the reference time) of the conditional averages in figure 16 is approximately inversely proportional to the integration time. Interpreting the time between the minimum and the maximum of the conditional averages in figure 12(a) as half a period, the integration time then is approximately 76% of the period. For this and other moderate integration times the results are comparable with the result from the sine-wave example in §2.2. The quantity $n_{\mathrm{pos}}(T)$ can thus be interpreted as a frequency of occurrence of events (to be compared with the concept of bursting frequency) with timescales about 30% larger than T. The timescale distribution of the events is obtained from plots as those in figures 8 and 9, where events are seen to be found for a wide range of integration times. The pattern-recognition technique, used by Wallace *et al.* (1977), also identifies events with time scales varying over a wide range. There is a factor of about 25 between the smallest and the largest timescale contributing to their ensemble averages. Kim, Kline & Reynolds (1971) have already pointed out that one should think of a dominant band of length- or time-scales (for the events) rather than a single sharply defined value.

It has long been debated whether the mean time between bursts (or events) scales with inner or outer variables (see e.g. Laufer & Badri Narayan 1971). All definitions of the mean time between events contain a good deal of subjectivity. One might even question the value of this concept owing to the difficulty of finding an objective definition. For both the VITA technique (as shown in this study) and for the uv-quadrant method (as shown by Sabot & Comte-Bellot 1976) the number of events detected decreases rapidly with increasing threshold level. The frequency of occurrence of (or mean time between) events is therefore a strong function of the threshold level, and for the VITA technique it is also a function of the integration time. Also for visual studies related problems exist. A method to investigate which timescales are the governing ones for the duration and frequency of occurrence of the events is to examine which timescales should be used for normalization to make the curves $n_{\mathrm{pos}}(T)$ (or $n_{\mathrm{neg}}(T)$) collapse for different Reynolds numbers (for the same threshold level). In figure 9 ($y^+ = 13$) outer scaling has been used. This type of scaling was found to be appropriate far from the wall. It should be noted that also the frequency spectra in the outer region can be made to collapse with outer scaling. At for example $y^+ = 13$, and closer to the wall, discrepancies appear for short integration times with this scaling. However, small timescales are often associated with small lengthscales and for spanwise lengthscales of the same order of magnitude as the length of the probe, effects of spatial averaging become important. The same probe was used in this study for all Reynolds numbers, and its length corresponds to approximately 32 viscous length units for the highest Reynolds number. This cannot be considered as small compared with the smallest scales of the turbulence, so nothing definite can be said about the scaling for very small timescales.

Conditional averages depend strongly on the method used. For the VITA method some single realizations (figure 13) can be compared with the ensemble averages in figure 12. A strong coherence is seen close to the reference time. However, at large distances in time relative to the reference time the events are uncorrelated, and hence the value of the conditionally averaged quantity should tend to the long-time average. The sharp acceleration at the reference time as seen in the single events and the conditional average could be interpreted as being caused by an internal shear layer.

Theoretical modelling of such structures is discussed by Landahl (1980). The u-signal patterns during ejections and sweeps, reported by Comte-Bellot, Sabot & Saleh (1979), show little resemblance with the conditional averages obtained with the VITA technique. There are several possible explanations for this. The two detection schemes may detect distinctly different types of events or the effect may be due to the different ways of setting the reference time. The results of Blackwelder & Kaplan (1976) show a strong uv-activity during the events, but with an ensemble average of uv that is very small at the reference time. Some work on the similarities and differences in the information obtained with different detection schemes is reported by Offen & Kline (1975) and by Eckelmann & Wallace (1981). Further work in this area is highly desirable.

5. Summary

(i) Measurements of the first four statistical moments at three Reynolds numbers are presented that complement and extend the results of previous turbulent channel-flow studies.

(ii) The structures detected with the VITA technique are similar at all Reynolds numbers studied, and their appearance is correlated with the skewness and flatness factors (figures 14 and 15).

(iii) The VITA technique has a band-pass-filter character, and the relation between the integration time and the duration of the detected events is illustrated by for example the conditional averages computed for different integration times in figure 16.

(iv) Separation of the two types of events, accelerations and retardations, makes the conditional averages collapse for a wide range of threshold levels if the velocity is scaled with $(ku_{\mathrm{rms}}^2)^{\frac{1}{2}}$.

(v) The retardations have a duration typically several times as large as that of the accelerations (figure 8).

(vi) The number of events decreases exponentially with the threshold level, and the events with large amplitude nearly always correspond to accelerations (figure 7).

(vii) The frequency of occurrence and the duration of the events scale with outer variables in the outer region of the flow.

The work reported here is part of a research program sponsored by the Swedish Maritime Research Centre (SSPA). We gratefully acknowledge this support. We also want to thank Professor M. T. Landahl for helpful suggestions during the work, Professor E. R. Lindgren, who took part in the original design and construction of the water tunnel, Dr H. Eckelmann, who helped us get started with the hot-film measurements, and Professor F. H. Bark for reading the manuscript and for numerous lunch-break discussions.

REFERENCES

Antonia, R. A. 1981 *Ann. Rev. Fluid Mech.* **13**, 131.

Blackwelder, R. F. & Kaplan, R. E. 1976 *J. Fluid Mech.* **76**, 89.

Bullock, K. J., Cooper, R. E. & Abernathy, F. H. 1978 *J. Fluid Mech.* **88**, 585.

Clark, J. A. 1968 *Trans. A.S.M.E.* D, *J. Basic Engng* **90**, 455.

Comte-Bellot, G. 1965 *Publications Scientifiques et Techniques du Ministère de l'Air* no. 419.

COMTE-BELLOT, G., SABOT, J. & SALEH, I. 1979 In *Proc. Dynamic Flow Conf. – Dynamic Measurements in Unsteady Flows*, 1978, *Marseille, Baltimore*, p. 213.

ECKELMANN, H. 1974 *J. Fluid Mech.* **65**, 439.

ECKELMANN, H. & WALLACE, J. M. 1981 In *The Role of Coherent Structures in Modelling Turbulence and Mixing* (ed. J. Jimenez). Lecture Notes in Physics, vol. 136, p. 292, Springer.

FAHLGREN, E. M., JOHANSSON, A. V. & ALFREDSSON, P. H. 1981 *R. Inst. Tech., Stockholm, Rep.* TRITA-MEK-81-01 (ISSN 0348-467 X).

JOHANSSON, A. V. & ALFREDSSON, P. H. 1981 *R. Inst. Tech., Stockholm, Rep.* TRITA-MEK-81-04 (ISSN 0348-467 X).

KIM, H. T., KLINE, S. J. & REYNOLDS, W. C. 1971 *J. Fluid Mech.* **50**, 133.

KREPLIN, H.-P. 1976 *Mitteilung aus dem MPI für Strömungsforschung und der AVA Göttingen* no. 63.

LANDAHL, M. T. 1980 In *Proc. ICHMT/IUTAM Symp. on Heat and Mass Transfer and Structure of Turbulence, Dubrovnik, Yugoslavia.*

LAUFER, J. 1951 *NACA Rep.* no. 1053.

LAUFER, J. & BADRI NARAYANAN, M. A. 1971 *Phys. Fluids* **14**, 182.

OFFEN, G. R. & KLINE, S. J. 1975 In *Proc. 3rd Symp. on Turbulence in Liquids*, 1973, *Univ. Missouri–Rolla* (ed. G. K. Patterson & J. L. Zakin), p. 289.

PERRY, A. E. & ABELL, C. J. 1975 *J. Fluid Mech.* **67**, 257.

RAO, K. N., NARASIMHA, R. & BADRI NARAYANAN, M. A. 1971 *J. Fluid Mech.* **48**, 339.

SABOT, J. & COMTE-BELLOT, G. 1976 *J. Fluid Mech.* **74**, 767.

WALLACE, J. M., BRODKEY, R. S. & ECKELMANN, H. 1977 *J. Fluid Mech.* **83**, 673.

WILLMARTH, W. W. 1975 *Adv. Appl. Mech.* **15**, 159.

WILLMARTH, W. W. & LU, S. S. 1972 *J. Fluid Mech.* **55**, 65.

ZARIČ, Z. 1972 *Adv. Heat Transfer* **8**, 285.

ZARIČ, Z. 1975 *Int. J. Heat Mass Transfer* **18**, 831.